CHINESE OPTICS LETTERS

Vol. 19, No. 12 | December 2021

Fine edge detection in single-pixel imaging

Liyu Zhou (周立宇), Xianwei Huang (黄贤伟), Qin Fu (付 芹), Xuanpengfan Zou (邹璇彭凡), Yanfeng Bai (白艳锋)*, and Xiquan Fu (傅喜泉)**

College of Computer Science and Electronic Engineering, Hunan University, Changsha 410082, China

*Corresponding author: yfbai@hnu.edu.cn

**Corresponding author: fuxq@hnu.edu.cn

Received April 25, 2021 | Accepted July 7, 2021 | Posted Online September 14, 2021

Typical single-pixel imaging techniques for edge detection are mostly based on first-order differential edge detection operators. In this paper, we present a novel edge detection scheme combining Fourier single-pixel imaging with a second-order Laplacian of Gaussian (LoG) operator. This method utilizes the convolution results of an LoG operator and Fourier basis patterns as the modulated patterns to extract the edge detail of an unknown object without imaging it. The simulation and experimental results demonstrate that our scheme can ensure finer edge detail, especially under a noisy environment, and save half the processing time when compared with a traditional first-order Sobel operator.

Keywords: single-pixel imaging; edge detection; Laplacian of Gaussian operator.

DOI: 10.3788/COL202119.121101

1. Introduction

Ghost imaging (GI), as a novel imaging technique, has received extensive attention in the field of quantum optics recently. Different from traditional imaging, GI is a nonlocal imaging technique that calculates spatial intensity correlation between two light beams to achieve the purpose of final imaging. GI was first, to the best of our knowledge, realized in an experiment by using entangled photon pairs in 1995[1,2]. Later, researchers found that the thermal source and pseudo-thermal source could also be used to implement GI[3–6]. To further simplify the experimental setup, the theoretical and experimental results have demonstrated that GI could be implemented only with a bucket detector by modulating the light source since 2008, which was also called single-pixel imaging (SPI)[7,8]. The initial SPI used random speckles. Then, it was found that Fourier basis patterns[9] and Hadamard basis patterns[10,11] with orthogonal properties could obtain better imaging effects. In recent years, various studies have shown that SPI can be applied to some important fields, such as three-dimensional imaging[12–14], fast-moving object tracking[15,16], and phase imaging[17–19].

In computer vision, edge detection is an important research field. Recently, much work on how to apply the advantage of SPI to the edge detection technique has been carried out[20–25]. In 2009, Jack *et al.* obtained edge enhanced images by use of nonlocal phase filters within a GI system[20]. Then, Liu *et al.* presented gradient GI in 2015. The method has better results by choosing a proper gradient angle based on prior knowledge of the imaging object[21]. One year later, speckle-shifting GI was proposed. By shifting the random speckles spatially, it can implement edge detection without any prior knowledge of the object[22]. In 2018, Ren *et al.* reported an edge detection scheme based on SPI in the frequency domain, which achieves a better SNR performance[23]. In 2020, Liu *et al.* achieved the edge detection of complex-valued objects by scanning spiral phase-encoded plane waves[25].

Note that most of the above works focused on the first-order differential edge detection operators, such as the Sobel operator, or the corresponding improved operators on this basis, and Mao *et al.* described that the second-order Laplacian operator could not achieve good results, which is different from the first-order Sobel operator[22]. So, there is a question whether second-order differential operators are suitable for SPI or not. In this paper, we present a new edge detection scheme that combines Fourier SPI (FSI) with the second-order Laplacian of Gaussian (LoG) operator[26] and call it LFSI. Comparative studies among the scheme that combines FSI with the Sobel operator, the scheme that uses the LoG operator to extract edge information after imaging an unknown object, and LFSI are performed. According to the simulation and experimental results, LFSI is feasible and can obtain finer edge information. In addition, it is also shown that LFSI has better noise robustness.

2. Principle

Figure 1 shows the experimental setup of LFSI. Inside the projector, a beam of white light from a light emitting diode (LED) lamp illuminates a liquid crystal display (LCD) that is controlled by a computer to generate the modulated patterns.

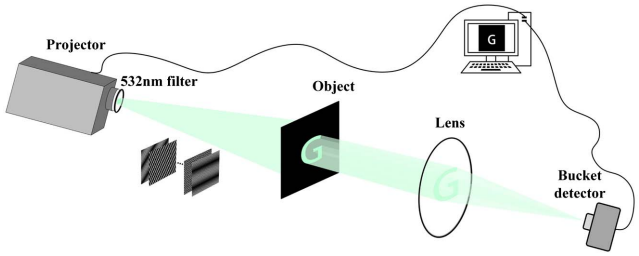

Fig. 1. Setup of LFSI.

The modulated light passes through a 532 nm filter placed in front of the projector lens and then illuminates the target object. Finally, all of the light transmitted by the object is collected by a lens and focused onto a bucket detector without spatial resolution. Edge information of an unknown object can be acquired through a two-dimensional (2D) inverse Fourier transform algorithm by a computer.

In the FSI, a series of 2D Fourier basis patterns with orthogonal properties are used as modulated patterns. The mathematical expression for each pattern is described as follows:

$$P_\phi(x,y,f_x,f_y) = a + bC_\phi(x,y,f_x,f_y), \tag{1}$$

where $C_\phi(x,y,f_x,f_y) = \cos(2\pi f_x x + 2\pi f_y y + \phi)$. (x,y) represents the 2D Cartesian coordinates in the spatial domain, and (f_x,f_y) represents the coordinates in the frequency domain. ϕ is the initial phase. a denotes the average image intensity, and b denotes the contrast. Generally, both a and b are 0.5. From Eq. (1), it can be seen that each pattern is determined by its spatial frequency (f_x,f_y) and initial phase ϕ. Thus, by sequentially projecting four patterns with different initial phase $(\phi = 0, \pi/2, \pi, 3\pi/2)$ onto the object O, the Fourier coefficient $I(f_x,f_y)$ of the object at a certain spatial frequency can be obtained:

$$\begin{aligned} I(f_x,f_y) &= \frac{1}{2b}\{[D_0(f_x,f_y) - D_\pi(f_x,f_y)] \\ &\quad + j[D_{\pi/2}(f_x,f_y) - D_{3\pi/2}(f_x,f_y)]\} \\ &= \frac{1}{2b}\iint_\Omega \mathrm{d}x\mathrm{d}y O(x,y)\exp[-j2\pi(f_x x + f_y y)] \\ &= \frac{1}{2b}\mathcal{F}[O](f_x,f_y), \end{aligned} \tag{2}$$

where $D_\phi(f_x,f_y) = \iint_\Omega \mathrm{d}x\mathrm{d}y O(x,y)P_\phi(x,y,f_x,f_y)$, which represents the light irradiance values recorded by the bucket detector. j is the imaginary unit, and Ω is the illuminated area. $\mathcal{F}$ denotes the Fourier transformation. By repeating the four-step phase-shifting method[27], the entire frequency spectrum of the object can be acquired. Finally, the 2D inverse Fourier transformation of the frequency spectrum is the object's spatial image.

Then, we discuss how to combine FSI with edge detection from two aspects. On the one hand, the edge detection of an image is often expressed as the convolution of the image and edge detection operators in the field of image processing. On the other hand, it can be found that when a convolution kernel satisfies some conditions, using the convolution kernel to perform a convolution operation on modulated speckles is equivalent to performing a corresponding convolution operation on the object's image according to Eq. (3):

$$\begin{aligned} &\iint_\Omega \mathrm{d}x\mathrm{d}y\{\exp[-j2\pi(f_x x + f_y y)] * h(x,y)\}O(x,y) \\ &= \iint_\Omega \mathrm{d}x\mathrm{d}y O(x,y) \\ &\quad \times \left\{\iint_\Omega \mathrm{d}x'\mathrm{d}y' \exp[-j2\pi(f_x x' + f_y y')]h(x-x', y-y')\right\} \\ &= \iint_\Omega \mathrm{d}x'\mathrm{d}y' \exp[-j2\pi(f_x x' + f_y y')] \\ &\quad \times \left[\iint_\Omega \mathrm{d}x\mathrm{d}y O(x,y)h(x-x', y-y')\right] \\ &= \iint_\Omega \mathrm{d}x'\mathrm{d}y' \exp[-j2\pi(f_x x' + f_y y')] \\ &\quad \times [O(x',y') * h(-x', -y')], \end{aligned} \tag{3}$$

where $*$ is the convolution operator, and h is the convolution kernel. From Eq. (3), it can be seen that as long as the edge detection operator as a convolution kernel satisfies the equation $h(x,y) = h(-x,-y)$, edge detection can be implemented by modifying the modulated pattern $P_\phi(x,y,f_x,f_y)$.

For the edge detection operator, there are the first-order differential operator and second-order differential operator. The first-order differential operator, such as the Sobel operator, is widely discussed in many works. Here, we focus on the second-order LoG operator, and the convolution kernel of the LoG operator can be written as

$$\mathrm{LoG}(x,y) = \frac{x^2 + y^2 - 2\sigma^2}{\sigma^4}\exp\left(-\frac{x^2 + y^2}{2\sigma^2}\right), \tag{4}$$

where σ is the standard deviation of Gaussian distribution, which is the difference between the LoG operator and the Laplacian operator[28]. As we know, the Laplacian operator is a second-order differential operator that can compute a digital approximation of the second derivative at every point in the target imaging. So, when noise in the environment exists, the edge detection results of the Laplacian operator are easily affected by the noise, while the LoG operator can reduce the noise interference caused by the second derivative of the image because it adds a Gaussian function to blur the target image on the basis of the Laplacian operator.

From Eq. (4), it is easy to find that the convolution kernel of the LoG operator is origin-symmetric and satisfies the equation $\mathrm{LoG}(x,y) = \mathrm{LoG}(-x,-y)$. So, Eq. (1) can be modified as follows:

$$Q_\phi(x,y,f_x,f_y) = a + b[C_\phi * \mathrm{LoG}](x,y). \tag{5}$$

Correspondingly, the Fourier coefficient $\tilde{I}(f_x,f_y)$ is expressed as

$$\begin{aligned}\tilde{I}(f_x,f_y) &= \frac{1}{2b}\iint_\Omega \mathrm{d}x\mathrm{d}y O(x,y) \\ &\quad \times \{\exp[-j2\pi(f_x x + f_y y)] * \mathrm{LoG}(x,y)\} \\ &= \frac{1}{2b}\mathcal{F}[O(x,y) * \mathrm{LoG}(-x,-y)] \\ &= \frac{1}{2b}\mathcal{F}[O * \mathrm{LoG}](f_x,f_y).\end{aligned} \tag{6}$$

Compared with Eq. (2), what the 2D inverse Fourier transformation of the new frequency spectrum denotes is not the object's image but the convolution of the image and edge detection operator. The results of $[O * \mathrm{LoG}](x,y)$ contain positive and negative values. Then, where the edge is can be determined by finding the position of the zero point between the positive and negative values, and this method is also called zero crossing. Therefore, by modifying the Fourier basis patterns, the edge information of an unknown object can be extracted directly without the need to get the object's spatial imaging.

Here, when LoG of Eq. (5) is replaced with the convolution kernel of the Sobel operator[28], we call it Scheme I. The scheme that images an unknown object first, and then uses the second-order LoG operator to implement edge detection, is called Scheme II. Both schemes will be compared with LFSI.

3. Numerical and Experimental Results

In this section, we carry out the numerical simulations and experiments to compare the performance of three edge detection schemes. The purpose of comparison is mainly to clarify three problems. The first one is whether SPI with the second differential operator is feasible to implement edge detection. The second one is whether the performance of combining FSI with the second-order LoG operator is better than that with first-order Sobel operator, as far as the results of edge detection are concerned. The third one is why we do not image an object firstly before extracting the edge information but utilize the LoG operator to modify the Fourier basis patterns to realize edge detection directly.

Without loss of generality, we use an 'HNU' binary object and a 'windmill' grayscale object with 64×64 imaging resolution in the presented simulation. To evaluate the results of edge detection qualitatively, the SNR is defined as[22]

$$\mathrm{SNR} = \frac{\mathrm{mean}(I_{\mathrm{edge}}) - \mathrm{mean}(I_{\mathrm{background}})}{\sqrt{\mathrm{var}(I_{\mathrm{background}})}},$$

where I_{edge} and $I_{\mathrm{background}}$ correspond to the intensity values of the edge detection results in the object's edge and background region, respectively.

Firstly, the performance of three schemes in a noise-free environment is discussed, as shown in Fig. 2. It is easy to find in

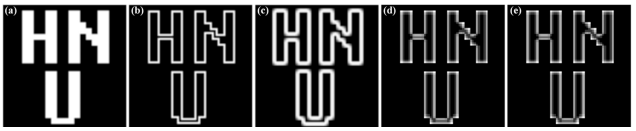

Fig. 2. Simulation results. (a) 'HNU' binary image. (b) Original edge image of (a). (c)–(e) The results of edge detection based on Scheme I, Scheme II, and LFSI, respectively.

Fig. 2(c) that the result of Scheme I presents thicker edges, while Scheme II and LFSI get finer edge detail, which corresponds to characteristics of the human visual system. Then, it can be seen that the results in Figs. 2(d) and 2(e) have no difference because no noise is considered. So, why we do not use Scheme II to implement edge detection? Besides, both the image and edge information of the object can be obtained at the same time in this way. What we want to discuss next focuses on this question. As we know, noise is inevitable during the practical application. So, we add different levels of white Gaussian noise into the modulated patterns[29] and the detection data in our simulation.

Figure 3 shows the simulation results of the binary object 'HNU' in different noise environments. From Figs. 3(b) and 3(c), it can be seen that regardless of light source noise or detection noise, the edge detection results of Scheme II are more likely to interfere when compared to LFSI. At the same time, Scheme I also shows good anti-noise performance [see Fig. 3(a)], while the thicker edge detail of Scheme I makes its SNR much smaller than that of LFSI. Besides, morphological processing is performed for the problem of noise in the edge image [see Fig. 3(c)]. Also, it is implemented by setting an appropriate threshold to binarize the edge images and then using the built-in function imclose of

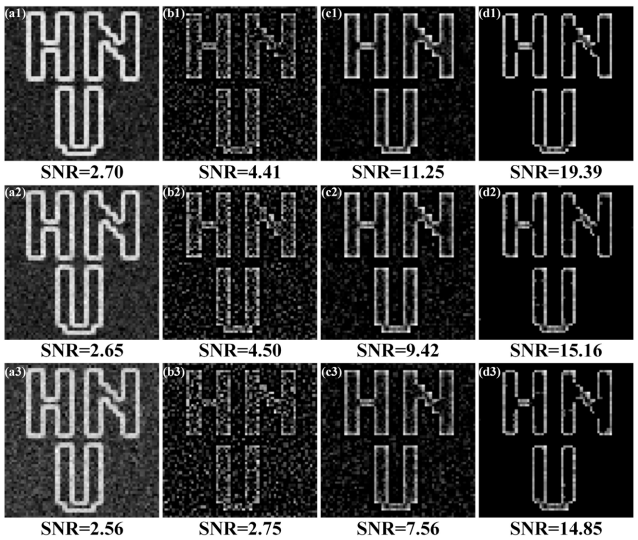

Fig. 3. Simulation results after adding noise. (a)–(c) Results of edge detection based on Scheme I, Scheme II, and LFSI. (d) Morphological processing results of (c). First row: adding SNR = 10 dB detection noise and no light source noise; second row: adding SNR = 10 dB light source noise and no detection noise; third row: adding SNR = 10 dB detection noise and light source noise.

MATLAB to process these binary images. It is easy to find that most of edge contour information is extracted from the edge image after morphological processing, which is confirmed from the increase of SNR in Fig. 3(d).

Next, a 'windmill' grayscale object is used to repeat the above simulation process. It is shown that the conclusions from Fig. 4 are similar with those from Fig. 3. Then, we further compare three edge detection schemes through experiments. The 'G' binary object and 'ghost' grayscale object are used as our test objects, the object's size is 52 mm × 52 mm, and the imaging resolution is 50 × 50. Due to the limit of the Nyquist measurement[30] and four-step phase-shifting method, there are 50 × 50 × 4 measurements for Scheme II to reconstruct the object's edge image. Benefitting from the rotation invariance of the LoG operator, the edge image of LFSI can be obtained with 50 × 50 × 4 measurements. However, the number of measurements for Scheme I is 50 × 50 × 4 × 2, which means that Scheme I takes twice as long as Scheme II and LFSI because the Sobel operator is divided into the x direction and y direction. In other words, the higher the imaging resolution is, the more time it takes. Here, the corresponding results are plotted in Fig. 5. The significant difference between the simulation and experimental results is that more periodic noise appears in Figs. 5(d1) and 5(d2). A reasonable explanation for this difference may originate from the noise considered. Especially, we find that the intensity of light source projected from our single-LCD projector does not linearly correspond to the change of the gray value of the modulated patterns, which may introduce the periodic noise in Scheme II. Nevertheless, the results in Figs. 5(e1) and 5(e2) are not too affected by this interference. From the above results, it can be drawn that LFSI has better performance than other schemes, which is consistent with the simulations.

It is also noted that the SNRs of GI with the second-order Laplacian operator are almost zero in Ref. [22], while we get

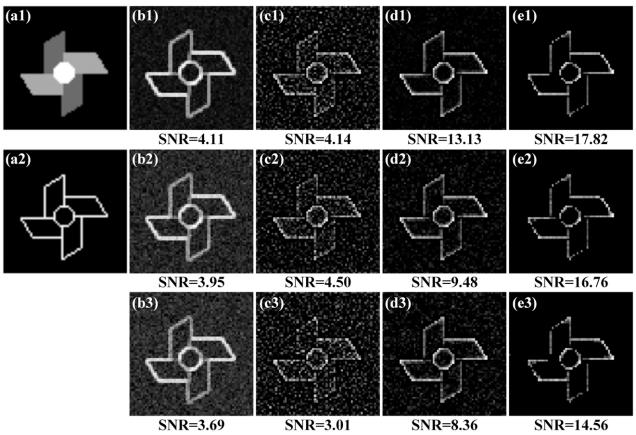

Fig. 4. Simulation results after adding noise. (a1), (a2) Original image and edge image of 'windmill' grayscale image. (b)–(d) Results of edge detection based on Scheme I, Scheme II, and LFSI, respectively. (e) Morphological processing results of (d). First row: adding SNR = 10 dB detection noise and no light source noise; second row: adding SNR = 10 dB light source noise and no detection noise; third row: adding SNR = 10 dB detection noise and light source noise.

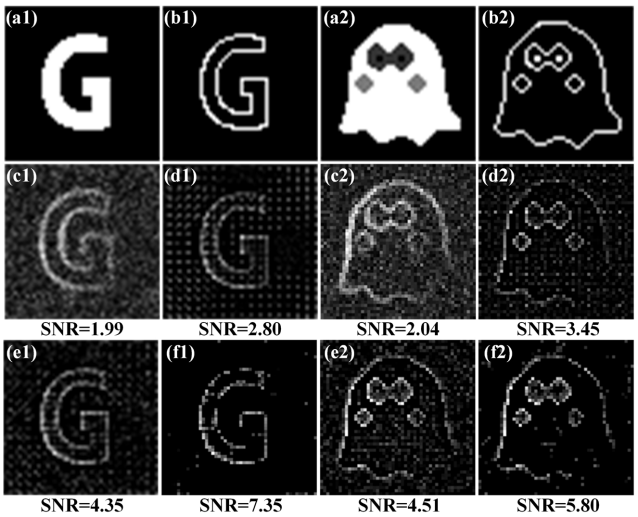

Fig. 5. Experimental results. (a1), (b1) Original image and edge of 'G' binary image. (a2), (b2) Original image and edge of 'ghost' image. (c)–(e) Experimental results of edge detection based on Scheme I, Scheme II, and LFSI, respectively. (f) Morphological processing results of (e).

good SNRs in LFSI. The difference may be explained as follows. First, the second-order Laplacian operator is more easily affected by the noise in contrast to the second-order LoG operator, as mentioned before. Second, LFSI uses Fourier basis patterns instead of the random speckles used in Ref. [22]. It has been proved that Fourier basis patterns are better than the random speckles on improving imaging quality when imaging an unknown object[9], and this conclusion is also applicable for edge detection. Finally, using the convolution results of the LoG operator and Fourier basis patterns as modulated patterns directly may reduce the experimental errors caused by shifting speckles.

4. Conclusion

In conclusion, we have developed an edge detection scheme combining the FSI technique with a second-order LoG operator. The simulation and experimental results clearly demonstrate that the second-order LoG operator can also be applied to SPI to implement edge detection. Besides, LFSI obtains finer edge information and saves half the processing time in contrast to the first-order Sobel operator. At the same time, the anti-noise performance of LSFI is better because of the Fourier basis patterns. Therefore, one potential application of our method is to obtain accurate edge information in microscopic imaging technology.

Acknowledgement

This work was supported by the National Natural Science Foundation of China (Nos. 61871431, 61971184, and 62001162) and China Postdoctoral Science Foundation (No. 2019M662767).

References

1. T. B. Pittman, Y. H. Shih, D. V. Strekalov, and A. V. Sergienko, "Optical imaging by means of two-photon quantum entanglement," Phys. Rev. A **52**, R3429 (1995).
2. D. V. Strekalov, A. V. Sergienko, D. N. Klyshko, and Y. H. Shih, "Observation of two-photon ghost interference and diffraction," Phys. Rev. Lett. **74**, 3600 (1995).
3. R. S. Bennink, S. J. Bentley, and R. W. Boyd, "'Two-photon' coincidence imaging with a classical source," Phys. Rev. Lett. **89**, 113601 (2002).
4. J. Cheng and S. S. Han, "Incoherent coincidence imaging and its applicability in X-ray diffraction," Phys. Rev. Lett. **92**, 093903 (2004).
5. F. Ferri, D. Magatti, A. Gatti, M. Bache, E. Brambilla, and L. A. Lugiato, "High-resolution ghost image and ghost diffraction experiments with thermal light," Phys. Rev. Lett. **94**, 183602 (2005).
6. A. Valencia, G. Scarcelli, M. D'Angelo, and Y. Shih, "Two-photon imaging with thermal light," Phys. Rev. Lett. **94**, 063601 (2005).
7. J. H. Shapiro, "Computational ghost imaging," Phys. Rev. A **78**, 061802 (2008).
8. Y. Bromberg, O. Katz, and Y. Silberberg, "Ghost imaging with a single detector," Phys. Rev. A **79**, 053840 (2009).
9. Z. B. Zhang, X. Ma, and J. G. Zhong, "Single-pixel imaging by means of Fourier spectrum acquisition," Nat. Commun. **6**, 6225 (2015).
10. L. Wang and S. M. Zhao, "Fast reconstructed and high-quality ghost imaging with fast Walsh–Hadamard transform," Photon. Res. **4**, 240 (2016).
11. J. H. Gu, S. Sun, Y. K. Xu, H. Z. Lin, and W. T. Liu, "Feedback ghost imaging by gradually distinguishing and concentrating onto the edge area," Chin. Opt. Lett. **19**, 041102 (2021).
12. B. Sun, M. P. Edgar, R. Bowman, L. E. Vittert, S. Welsh, A. Bowman, and M. J. Padgett, "3D computational imaging with single-pixel detectors," Science **340**, 844 (2013).
13. Z. B. Zhang and J. G. Zhong, "Three-dimensional single-pixel imaging with far fewer measurements than effective image pixels," Opt. Lett. **41**, 2497 (2016).
14. H. Z. Jiang, H. J. Zhai, Y. Xu, X. D. Li, and H. J. Zhao, "3D shape measurement of translucent objects based on Fourier single-pixel imaging in projector-camera system," Opt. Express **27**, 33564 (2019).
15. Z. B. Zhang, J. Q. Ye, Q. W. Deng, and J. G. Zhong, "Image-free real-time detection and tracking of fast moving object using a single-pixel detector," Opt. Express **27**, 35394 (2019).
16. Q. W. Deng, Z. B. Zhang, and J. G. Zhong, "Image-free real-time 3-D tracking of a fast-moving object using dual-pixel detection," Opt. Lett. **45**, 4734 (2020).
17. K. Ota and Y. Hayasaki, "Complex-amplitude single-pixel imaging," Opt. Lett. **43**, 3682 (2018).
18. Y. Liu, J. L. Suo, Y. L. Zhang, and Q. H. Dai, "Single-pixel phase and fluorescence microscope," Opt. Express **26**, 32451 (2018).
19. X. Y. Hu, H. Zhang, Q. Zhao, P. P. Yu, Y. M. Li, and L. Gong, "Single-pixel phase imaging by Fourier spectrum sampling," Appl. Phys. Lett. **114**, 051102 (2019).
20. B. Jack, J. Leach, J. Romero, S. Franke-Arnold, M. Ritsch-Marte, S. M. Barnett, and M. J. Padgett, "Holographic ghost imaging and the violation of a Bell inequality," Phys. Rev. Lett. **103**, 083602 (2009).
21. X. F. Liu, X. R. Yao, R. M. Lan, C. Wang, and G. J. Zhai, "Edge detection based on gradient ghost imaging," Opt. Express **23**, 33802 (2015).
22. T. Y. Mao, Q. Chen, W. J. He, Y. H. Zou, H. D. Dai, and G. H. Gu, "Speckle-shifting ghost imaging," IEEE Photon. J. **8**, 6900810 (2016).
23. H. D. Ren, S. M. Zhao, and J. Gruska, "Edge detection based on single-pixel imaging," Opt. Express **26**, 5501 (2018).
24. H. Guo, R. Y. He, C. P. Wei, Z. Q. Lin, L. Wang, and S. M. Zhao, "Compressed ghost edge imaging," Chin. Opt. Lett. **17**, 071101 (2019).
25. Y. F. Liu, P. P. Yu, X. Y. Hu, Z. Q. Wang, Y. M. Li, and L. Gong, "Single-pixel spiral phase contrast imaging," Opt. Lett. **45**, 4028 (2020).
26. D. Marr and E. Hildreth, "Theory of edge detection," Proc. R. Soc. Lond. B **207**, 187 (1980).
27. W. W. Meng, D. F. Shi, J. Huang, K. Yuan, Y. J. Wang, and C. Y. Fan, "Sparse Fourier single-pixel imaging," Opt. Express **27**, 31490 (2019).
28. R. C. Gonzalez and R. E. Woods, *Digital Image Processing*, 3rd ed. (Prentice Hall, 2007).
29. M. J. Sun, Z. H. Xu, and L. A. Wu, "Collective noise model for focal plane modulated single-pixel imaging," Opt. Lasers Eng. **100**, 18 (2018).
30. O. Katz, Y. Bromberg, and Y. Silberberg, "Compressive ghost imaging," Appl. Phys. Lett. **95**, 131110 (2009).